Received 22 January 2021; revised 25 February 2021; accepted 25 February 2021. Date of publication 3 March 2021; date of current version 15 March 2021.

Digital Object Identifier 10.1109/OJAP.2021.3063528

Penta-Band Inverted-F Antenna Tuned by High-Voltage Switchable RF Capacitors

VALENTYN SOLOMKO [1], OGUZHAN OEZDAMAR [2] (Graduate Student Member, IEEE), ROBERT WEIGEL [2] (Fellow, IEEE), AND AMELIE HAGELAUER [3] (Senior Member, IEEE)

[1]RF and Sensors, Infineon Technologies AG, 85579 Neubiberg, Germany
[2]Institute of Electronics Engineering, University of Erlangen-Nuremberg, 91058 Erlangen, Germany
[3]Chair of Communications Electronics, University of Bayreuth, 95447 Bayreuth, Germany

CORRESPONDING AUTHOR: O. OEZDAMAR (e-mail: oguzhan.oezdamar@fau.de)

ABSTRACT A penta-band inverted-F antenna (IFA) tuned by two high-voltage aperture tuning networks is presented in the paper. The design is based on a singe, non-bended radiating arm IFA. Each of the two aperture tuners comprises a high-voltage switchable RF capacitor IC in parallel with an off-chip inductor. The antenna can be tuned to any of the 5 bands of sub-4 GHz cellular spectrum between 690 MHz and 3800 MHz with return loss exceeding 6 dB at the feed over more that 95 % of the total frequency range. A systematic design and analysis of the penta-band IFA based on transmission line model is provided, tuning approach for carrier aggregation enablement over two bands at a time is discussed. A nonlinear performance of the designed antenna with RF capacitors fabricated in bulk-CMOS RF-switch technology is demonstrated.

INDEX TERMS Antenna tuning, aperture tuning, C-tuner, carrier aggregation, cellular user equipment, harmonics, high-voltage RF switch, inverted-F antenna, mobile handset, RF switch, switchable capacitor, user terminal.

I. INTRODUCTION

CAPACITIVELY loaded inverted-F antennas (IFAs) for mobile telephone handsets have been introduced more than two decades ago [1]. Capacitive loading reduces the resonance length of antenna providing reasonable radiation efficiency at low cellular frequency band even for compact structures. Recent advances in highly-linear, high-voltage tunable RF components enabled *variable* capacitive loading of the IFAs. Matching and radiation efficiency of such antennas could be fine-tuned to the specific frequency band while sustaining low level of nonlinear distortions required for co-existence of modern radio techniques, for example, carrier aggregation [2].

The sub-4 GHz cellular frequency spectrum, offering a good tradeoff between the coverage and capacity for cellular services [3], can be divided into 5 frequency ranges (bands): 690 MHz – 960 MHz (LB), 1420 MHz – 1520 MHz (LMB), 1710 MHz – 2200 MHz (MB), 2300 MHz – 2690 MHz (HB), 3300 MHz – 3800 MHz (UHB). For efficient space usage in a mobile phone operating in modern cellular networks it is desirable that a tunable inverted-F antenna covers multiple or all ranges, not necessarily at the same time.

In this work we focus primarily on *single, non-bended radiating arm* IFA topologies tuned by RF capacitors, as they are the most basic and practically applicable structures in cellular mobile devices [4]. In [5], two antenna demonstrators, each covering only one band – LB or HB – are reported. The antennas are aperture-tuned by a single RF-MEMS-based capacitor. Another IFA tuned within MB by means of a silicon varactor placed along a single radiating arm is presented in [6].

In one of the previous works the authors demonstrated a dual-band IFA tuned by an LC network based on a single RF capacitor [7]. The feed was matched at LB and MB. Shifting the same network further towards an open-end of the IFA would provide coverage of LB and HB (instead of MB). Addressing all three bands LB, MB and HB with a single aperture tuning capacitor seemed to be infeasible. The same tuning concept based on a digitally-controlled capacitor and a shunt inductor attached to the open end of a bended IFA

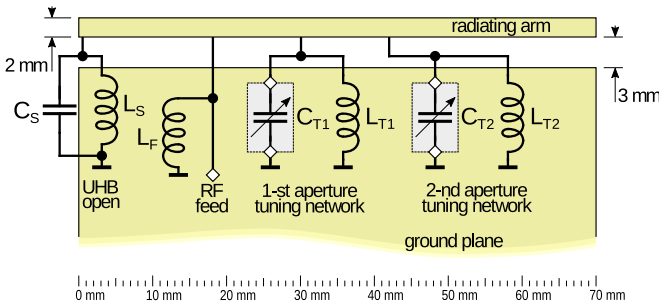

FIGURE 1. Proposed penta-band tunable inverted-F antenna.

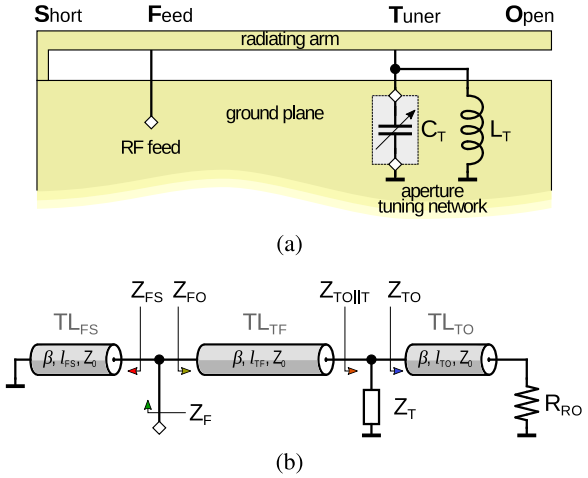

FIGURE 2. (a) – layout of the tuned single-arm IFA and (b) – its equivalent circuit based on the transmission line model of IFA.

arm over a compact ground plane is published in [8], where the antenna was covering LB frequency range.

A tuning topology reported in [9] besides a high-voltage switchable RF capacitor has additionally incorporated an RF switch at the feed, which allowed covering three bands, meaning LB, LMB and MB. A triple-band antenna integrated in a metallic back cover mobile phone mock-up presented in [4] is tuned by *three* MEMS-based aperture tuning capacitors. Each of the three capacitors is responsible for tuning the respective frequency band LB, MB or HB. Finally, an adjustable single-arm IFA covering three bands – LB, MB and HB – and tuned by a single switchable capacitor is presented in [10]. However, the radiating element of the IFA incorporates two section, the long one for exciting resonant modes at LB and HB, and the short one radiating at MB.

In this paper we propose a single-arm tunable IFA covering 5 bands mentioned above using two high-voltage switchable RF capacitors for aperture tuning. The UHB coverage is achieved by utilizing a short section of the radiating element, similarly to the MB resonant mode demonstrated in [10]. The final configuration of the proposed tunable antenna is shown in Fig. 1.

Among the novel aspects presented in the paper are:

- a systematic design and analysis of a tunable, single-arm IFA *based on transmission line model* is provided;
- tuning approach for independent and simultaneous coverage of two bands at a time is discussed;
- nonlinear performance of the designed antenna with two switchable RF capacitors in bulk-CMOS technology is demonstrated.

II. DESIGN OF PENTA-BAND TUNABLE IFA

We start the design by analysing how to tune a basic inverted-F antenna to each of the target bands separately, then we combine the findings to construct an antenna with five-band coverage. The layout of the basic single-arm IFA and an aperture tuning network directly coupled between the radiating element and ground plane are shown in Fig. 2(a). The radiating element and the ground plane are designed in a single 35-μm thick copper layer on a 1-mm FR4 substrate. The outer dimensions of the structure are 70 mm$\times$134 mm, which represents the size of a typical smartphone (only an upper part of the 129 mm long ground plane is shown in the figure).

The aperture tuning network is constructed as a parallel LC tanc, where C_T is a 5-bit switchable RF capacitor tuned between 450 fF and 2.7 pF with a uniform step size of 72 fF and L_T is a 27 nH SMD high-Q inductor. The reason for adding a parallel inductor to the aperture tuner is twofold:

- it can resonate out the shunt capacitance at LB frequencies, thus relaxing the requirements for the minimum capacitance of C_T;
- it protects the integrated circuit C_T from the damage during system-level ESD stress.

For the following analysis of tuning behavior of the antenna we use a transmission line model of a single-arm IFA [1], shown in Fig. 2(b). The model consists of three individual transmission lines TL_{FS}, TL_{TF} and TL_{TO} representing the respective sections of the radiating arm near the ground plane, the resistance R_{RO} modeling the radiation and loss resistance of the antenna [14], and the shunt impedance Z_T representing the aperture tuning network. The model is valid for estimating impedances along the radiating element of antenna, thus providing a simple tool for systematic design and analysis of the antenna tuning concept. The parameters of the model listed in Table 1 are extracted from a 3D-EM simulation of the planar antenna dimensioned as shown in Fig. 1. The reader is referred to authors' previous paper [14], where the extraction method is described in detail.

The impedance at the feed Z_F can be derived from the transmission line model using the following set of equations [11]:

$$Z_F = Z_{FS} \| Z_{FO}, \tag{1}$$

$$Z_{FS} = jZ_0 \tan \beta l_{FS}, \tag{2}$$

$$Z_{FO} = Z_0 \frac{Z_{TO\|T} + jZ_0 \tan \beta l_{TF}}{Z_0 + jZ_{TO\|T} \tan \beta l_{TF}}, \tag{3}$$

TABLE 1. Parameters of the transmission line model in Fig. 2(b).

Parameter	Value
Z_0 – characteristic impedance of transmission lines	121 Ω
β – propagation constant at $f = m{\cdot}900$ MHz	$m \cdot 31.9$ rad/m
l_{FS} – length of the transmission line feed-short	18 mm
$l_{TF} + l_{TO}$ – length of the section feed-open	52 mm
R_{RO} – radiation and loss resistance	800 Ω

$$Z_{TO\|T} = Z_{TO} \| Z_T, \tag{4}$$

$$Z_{TO} = Z_0 \frac{R_{RO} + jZ_0 \tan \beta l_{TO}}{Z_0 + jR_{RO} \tan \beta l_{TO}}. \tag{5}$$

Z_T represents the impedance of the aperture tuning network L_T–C_T:

$$Z_T = \frac{j\omega L_T}{1 - \omega^2 L_T C_T} \tag{6}$$

Note that the radiation resistance R_{RO} is the only resistive element in the transmission line model, meaning that if there is no impedance mismatch at the feed, all the power is dissipated at R_{RO} and antenna operates at its maximum efficiency.

We further visualize the impedance transformation (1)–(6) on the Smith Charts to demonstrate how the position of the tuner defines the frequency range that antenna is able to cover. Note, that since Z_T represents the tuner impedance and can take on different values, a single curve on the Smith Chart splits into multiple curves once reaching the point where Z_T is attached to.

A. LB TUNING

The untuned IFA produces a quarter-wavelength resonant mode at around 730 MHz with return loss of above 10 dB at the feed point. The frequency of the quarter-wave resonance is primarily defined by the length of the radiating arm, which is chosen to represent the size of a typical smartphone. An LC aperture tuning network, which is configured to exhibit a parallel resonance within LB, varies the effective electrical length of the radiating stripe, thus shifting the match at the feed depending on the capacitor settings. The tuner can be placed almost anywhere between the feed and open end. The exact position, however, impacts the tuning sensitivity and the return loss at the feed, as will be demonstrated next.

Fig. 3 shows the impedance transformation in the transmission line model for two different positions of the tuner: 20 mm and 30 mm away from the feed point ($l_{TF} = 20$ mm and $l_{TF} = 30$ mm respectively). For convenience of graphical representation of impedance transformation by the transmission lines, the reference impedance for all Smith Charts is set to the characteristic impedance of the transmission lines in the model, meaning to $Z_0 = 121\ \Omega$. Only one quarter of the complete LB frequency range is shown on the Chart to avoid crowding of the curves.

The TL_{TO} section moves the impedance Z_{TO} to the south of the Chart, which is then spread over the capacitive region

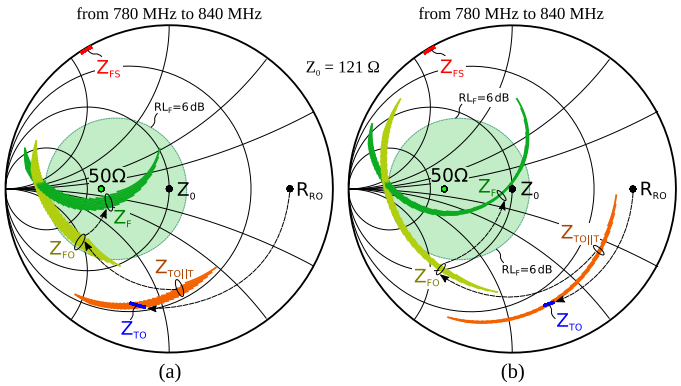

FIGURE 3. Impedance transformation in LB-tuned IFA when the tuner is attached to radiating element (a) – 20 mm away from feed and (b) – 30 mm away from feed. Reference impedance for the Smith Charts is $Z_0 = 121\ \Omega$.

as the capacitor in the tuner is swept between 450 fF and 2.7 pF with the step of 72 fF (in total 32 curves corresponding to impedance $Z_{TO\|T}$ are shown on the Charts). The spread is larger in Fig. 3(b), where the aperture tuner is placed closer to the open end of the IFA, resulting in a higher tuning sensitivity when the tuner is placed at the high-impedance region of the IFA. This finding has been experimentally proven in [12].

The transmission line TL_{TF} moves the 32 curves clockwise towards the low-impedance capacitive region of the Chart Z_{FO}. Finally, the inductive impedance Z_{FS} resonates out the capacitive part of Z_{FO}, bringing the impedance at the feed point into the 6 dB return loss region marked by a green circle around 50 Ω point of the Smith Chart.

From Fig. 3 the following can be concluded:

- placing the tuner at either one of the points, 20 mm or 30 mm away from feed, allows achieving target return loss of at least 6 dB at the feed;
- placing the tuner closer to the open end of the IFA results in higher tuning sensitivity.

B. LMB AND MB TUNING

At mid-band the tuner is placed 20 mm away from the feed, at the point where impedance Z_{TO} looking into the open end is inductive, see Fig. 4(a). The aperture tuner at LMB and MB operates predominantly above the parallel resonance, resulting in capacitive impedances Z_T, which transform the impedance Z_{TO} downwards the Chart along the imaginary axes, generating a set of curves $Z_{TO\|T}$. After a quarter-wavelength transformation by the transmission line TL_{TF}, the impedance Z_{FO} is combined in parallel with Z_{FS}, which appears at the high-ohmic inductive region of the Smith Chart. The resultant reflection coefficient curves at the feed cross the green RL_F circle, indicating a match to 50 Ω at the demonstrated frequency range between 1880 MHz and 2000 MHz.

C. HB TUNING

The optimal position of the tuner for MB, meaning 20 mm away from feed, unfortunately does not allow to

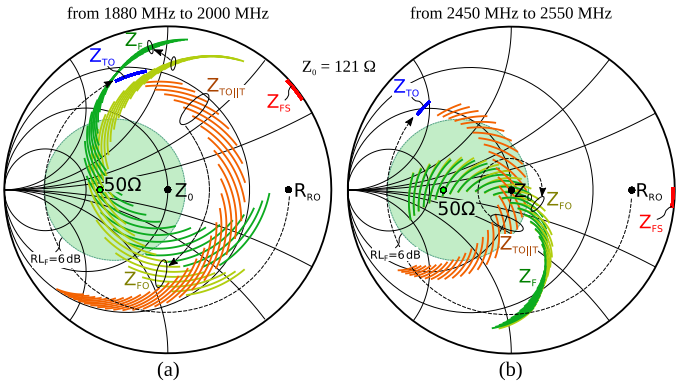

FIGURE 4. Impedance transformation (a) – in MB-tuned IFA when the tuner is attached to radiating element 20 mm away from feed and (b) – in HB-tuned IFA when the tuner is attached to radiating element 30 mm away from feed. Reference impedance for the Smith Charts is $Z_0 = 121\ \Omega$.

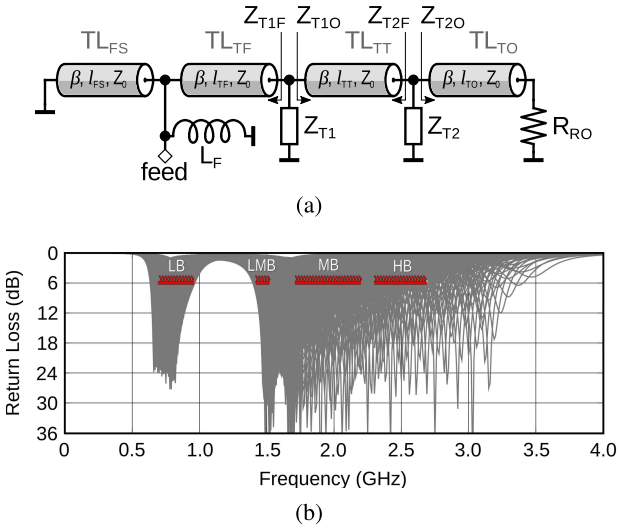

FIGURE 5. (a) – model of the quad-band IFA and (b) – calculated return loss at the feed for $l_{TF} = 12$ mm and $l_{TT} = 10$ mm (the values of other parameters of the model are listed in Table 1).

accommodate for high-band tuning. In order to address this band the tuner shall be moved closer to the open end, so that TL_{TF} could shift the R_{RO} by the same or even smaller phase angle than it does in MB case. Numerical evaluation of (1) reveals that $l_{TF} = 30$ mm is the optimal physical distance between the feed and the aperture tuner for covering HB. The Smith Chart in Fig. 4(b) demonstrates the HB tuning case within the frequency range of 2450 MHz – 2550 MHz.

D. QUAD-BAND TUNING TOPOLOGY

The IFA tuned by a single LC-tanc attached to the radiating element is capable of achieving up to triple-band coverage, with either LB-LMB-MB or LB-HB band combinations. It cannot, however, address MB and HB with the same electrically-tuned antenna.

For this reason two identical, independently-controlled tuners are placed at different points of antenna to achieve quad-band frequency coverage, meaning LB-LMB-MB-HB. The tuners can not be placed exactly at the locations identified in Sections II-B and II-C because of double loading of the IFA. We have used a model of the quad-band tunable IFA shown in Fig. 5(a) to obtain the appropriate locations for the tuners.

Z_{T1} and Z_{T2} represent the impedances of the aperture tuning networks defined as:

$$Z_{Ti} = \frac{j\omega L_{Ti}}{1 - \omega^2 L_{Ti} C_{Ti}}, \tag{7}$$

where $i \in \{1, 2\}$, $L_{Ti} = 27$ nH, C_{T1} and C_{T2} are independently-tuned in the range 450 fF – 2.7 pF with a uniform step of 72 fF. The shunt inductance L_F is added to account for the influence of an ESD protection element at the feed required in a real IFA implementation.

In order to find the proper location for the aperture tuners for best coverage of four bands defined above, we define and solve a numerical optimization task for the circuit in Fig. 5(a). The voltage standing wave ratio (VSWR) at the feed can be analytically found using the mathematics from Section II:

$$\gamma_F = \frac{1 + |(Z_F - Z_{0.FE})/(Z_F + Z_{0.FE})|}{1 - |(Z_F - Z_{0.FE})/(Z_F + Z_{0.FE})|}, \tag{8}$$

where $Z_{0.FE}$ is the reference impedance of the RF front-end electronics interfacing the antenna feed, typically 50 Ω.

In general, γ_F is a function of frequency, common transmission line properties β and Z_0, length of the individual transmission lines (defining the positions of the tuners) and states of the tuners (defining Z_{T1} and Z_{T2}). In particular, we have previously set the numerical values for all parameters, with l_{TF} and l_{TT} remaining to be unknown. For any arbitrary frequency point and fixed l_{TF} and l_{TT} we define the minimum VSWR at the feed over all possible tuning states:

$$\min_{C_{T1}, C_{T2}} \{\gamma_F\} \tag{9}$$

We then integrate (9) over frequency bands of interest:

$$OF = \int_{F_b} \min_{C_{T1}, C_{T2}} \{\gamma_F\} df, \tag{10}$$

where $F_b = f_{LB} \cup f_{LMB} \cup f_{MB} \cup f_{HB}$ is a union of specified frequency intervals. The expression (10) quantifies the ability of the tunable IFA to provide the impedance match at the feed point over the target frequency bands. The lower the OF is, the more beneficial is the tuning configuration. Therefore, we use (10) as an objective function for numerical optimization of the quad-band IFA model. The optimization problem is set as:

$$\min_{l_{TF}, l_{TT}} \{OF\}, \tag{11}$$

where l_{TF} and l_{TT} are the input arguments to be found, that bring the objective function to its minimum.

It is worth noting, that from the three known scalar quantities describing the mismatch power loss, namely, return loss, scalar reflection coefficient and VSWR, the latter is

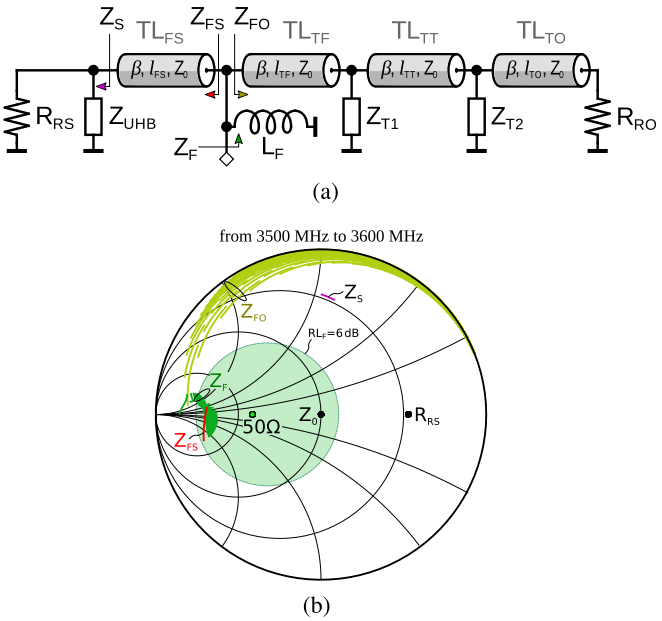

FIGURE 6. (a) – equivalent circuit of the penta-band IFA, (b) – impedance transformation in UHB.

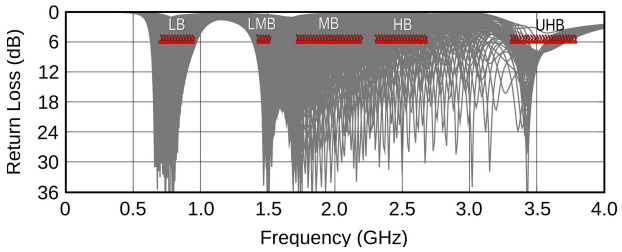

FIGURE 7. Calculated return loss at the feed of the circuit in Fig. 6(a).

the most appropriate for defining the objective function (10). VSWR, being by definition a Möbius transformation of the scalar reflection coefficient, nonlinearly grows the *OF* as the reflection at the feed goes away from zero. Such behavior of the VSWR function ensures that the *OF* does not mask the strongly-mismatched points in the response of the tuned IFA, discarding any inappropriate tuning configuration.

After solving the optimization problem (11) we have identified the optimal values for the input arguments: $l_{TF} = 12\,\text{mm}$ and $l_{TT} = 10\,\text{mm}$. The resultant return loss curves for these positions of the tuners are plotted in Fig. 5(b). There are in total $2^5 \cdot 2^5 = 1024$ curves for all possible states of the two 5-bit switchable capacitors.

E. PENTA-BAND TUNING TOPOLOGY

The impedance Z_{FO} of the radiating stripe at the feed point looking into the open end of the IFA is predominantly inductive and high-ohmic at the UHB frequencies and can not be matched to achieve reasonable power transfer to the feed. This is demonstrated in Fig. 6(b), where the reflection coefficient curves corresponding to Z_{FO} at 3500 MHz – 3600 MHz are plotted along the north periphery of the Smith Chart. It is worth mentioning, that the transmission line model is expected to be less accurate at UHB than at low-GHz frequencies.

In order to cover UHB, the section TL_{FS} of the IFA radiating arm is utilized – an approach similar to the one reported in [10], where the short section of the IFA was used to excite the quarter-wavelength resonant mode at 1800 MHz. In the quad-band topology one side of the TL_{FS} is shorted to ground. A parallel LC resonant tank has been attached to TL_{FS} instead of the short to sustain the quad-band coverage and complement it with the UHB. The circuit diagram is shown in Fig. 1, where said LC tank is denoted as "UHB open", with $L_S = 1.8\,\text{nH}$ and $C_S = 0.8\,\text{pF}$. The tank exhibits low reactive impedance at frequencies below 2700 MHz and approaches parallel resonance at UHB.

The equivalent circuit diagram of the penta-band IFA is shown in Fig. 6(a). Here, $Z_{UHB} = j\omega L_S/(1-\omega^2 L_S C_S)$ is the impedance of the LC tank, $R_{RS} = 400\ \Omega$ is the radiation and loss resistance of the IFA short section, analogous to R_{RO}. The numerical value for R_{RS} has been extracted from the 3D-EM simulated model of the IFA at 3.5 GHz. The numerical values for all other elements of the model remain identical to quad-band configuration.

At 3500 MHz the impedance Z_S is inductive and the electrical length of the section TL_{FS} is $1.4\frac{\lambda}{4}$, which bring the impedance Z_{FS} into the $RL_F = 6$ dB circle. As mentioned previously, Z_{FO} and $j\omega L_F$ are high-ohmic inductive impedances in parallel to Z_S, resulting in feed impedance Z_F which is mostly inside the target 6 dB return loss circle, see Fig. 6(b).

The return loss at the feed of the designed penta-band IFA for all 1024 tuning states is demonstrated in Fig. 7. The response is similar to quad-band structure up to 3 GHz and at UHB the design exhibits 6 dB return loss over most of the target frequency band.

It is worth noting, that the considered model of the IFA in Fig. 6(a) does not contain any lossy elements besides radiation resistances R_{RO} and R_{RS}, therefore return loss trend in Fig. 7 shall match with the antenna radiation efficiency.

F. ANTENNA CONTROL FOR CARRIER AGGREGATION

The penta-band antenna can be fine-tuned to at least one frequency within the five bands. In order to accommodate for carrier aggregation (CA) usage, multiple frequency bands shall be covered at the same time [13]. It is not straightforward to predict at which frequency combinations the impedance match at the feed can be achieved for the designed penta-band antenna without the complete numerical sweep over all tuner combinations. The following analysis is aimed at providing an estimation at which bands the simultaneous impedance match at the feed can potentially be expected.

Once the mechanical configuration of the tuned IFA is defined and fixed, the VSWR at the feed is transformed (simplified) into a function of two variables, C_{T1} and C_{T2},

TABLE 2. Normalized numerical aperture tuning sensitivity values according to (15) for the IFA model in Fig. 6(a).

	Directional vector $\mathbf{c}$ for (14)			
	$(1,1)$	$(1,-1)$	$(1,0)$	$(0,1)$
$S_{int}^{(LB)}/S_{int}^{(LB)}$	1	1	1	1
$S_{int}^{(LMB)}/S_{int}^{(LB)}$	1.2	–3.3	4.1	–0.1
$S_{int}^{(MB)}/S_{int}^{(LB)}$	2.5	–3.5	6.5	0.9
$S_{int}^{(HB)}/S_{int}^{(LB)}$	4.9	5.1	4.7	5.0

and frequency:

$$\gamma_F(\mathbf{C_T}, f), \tag{12}$$

where $\mathbf{C_T} = (C_{T1}, C_{T2})$ is a vector of arguments representing the capacitance of the tuners. Within the specified frequency band the best impedance match at the feed is achieved at a frequency point, where VSWR reaches its minimum:

$$f_m(\mathbf{C_T}) = \underset{f}{\operatorname{argmin}} \ \{\gamma_F(\mathbf{C_T}, f)\} \tag{13}$$

We assume that (13) is defined only if f_m does not lie on the boundary of the frequency interval representing the respective band, meaning that f_m belongs to the open frequency interval.

We introduce a scalar *aperture tuning sensitivity* function defined as a directional derivative of the best-match frequency point along a vector $\mathbf{c}$:

$$S(\mathbf{C_T}) = \nabla_{\mathbf{c}} f_m(\mathbf{C_T}) \tag{14}$$

The function (14) may be undefined for some intervals or subsets of $\mathbf{C_T}$ from the complete aperture tuning (AT) space for the reason that f_m may not be always defined as mentioned earlier.

We define the integral sensitivity over the complete aperture tuning space (A_T) as:

$$S_{int} = \frac{1}{A_T} \cdot \int_{A_T} S(\mathbf{C_T}) d^2\mathbf{C_T}. \tag{15}$$

The function (15) has been numerically evaluated for the designed penta-band tunable antenna in Fig. 6(a). The sensitivity for each of the four bands (except UHB, which is not tuned by the RF capacitors) has been calculated and normalized to the sensitivity in low-band for the ease of comparison. The derivatives have been calculated along the four different directional vectors $\mathbf{c}$, as listed in the Table 2. For example, the sensitivity for $\mathbf{c} = (1, -1)$ means the rate of change in best-match frequency when the first capacitor C_{T1} is tuned up in the value and second capacitor C_{T2} is tuned down.

The following can be observed and concluded:

- $\mathbf{c} = (1,\ 1)$: increase of the values of both tuning capacitors at the same time shifts the matching frequency at all bands in the same direction but with different speed (faster for high frequencies, as expected). Such tuning scenario *alone* does not provide enough flexibility for achieving wide CA coverage due to correlation in the shift of matching frequency;
- $\mathbf{c} = (1, -1)$: changing the capacitance values for the tuners in different directions exhibits negative sensitivity in LMB and MB with respect to LB. This means, that it is possible to shift the match at LMB and MB towards higher frequencies, while moving the LB match to the lower frequencies. Such tuning scenario, *together* with $\mathbf{c} = (1,\ 1)$, provides a high degree of freedom for a simultaneous and arbitrary match at LB–MLB or LB-MB, enabling CA usage for mentioned band combinations;
- CA in HB and LB can unlikely be efficiently addressed by the design for the same reason mentioned in the first bullet point.

The UHB is not included in the analysis for its low sensitivity to the aperture tuning. The suitability of the designed penta-band tunable antenna for CA support will be demonstrated in the following section.

III. EXPERIMENTAL RESULTS

The designed single-arm IFA tuned by two high-voltage switchable capacitors has been implemented in hardware. The photograph of the prototype is shown in Fig. 8. The demonstrator is based on a mechanically-reconfigurable inverted-F antenna, which has been described by the authors in detail in one of the previous publications [14]. In addition to penta-band antenna we have also assembled a quad-band modification (not shown in the figure), which comprises a metal short instead of the $L_S - C_S$ UHB open.

The 5-bit switchable RF capacitors C_{T1} and C_{T2} have been designed and fabricated in Infineon 130 nm bulk-CMOS switch process. The capacitors can be tuned in the range of $C_{min}/\Delta C/C_{max} = 450\,\text{fF}/72\,\text{fF}/2.7\,\text{pF}$ at low-band frequencies, with the Q-factor between 20 and 30 depending on the state at said band. The parts are designed for maximum 80 V RF voltage handling capabilities. Such voltage handling provides sufficient margin for practical large-signal operation – the maximum RF voltages against ground at the mounting points of the aperture tuners are expected not to exceed 70 V [14]. The circuit design of the RF capacitors is outside the scope of the paper, therefore the reader is referred to [15] for detailed description of a similar IC.

The two identical aperture tuning networks based on the switchable RF capacitor, as well as the UHB LC network, are mechanically attached to the carrier board. The capacitors are individually controlled from a shared two-wire interface, the total amount of tuning states is $2^{5+5} = 1024$, where 5 denotes the resolution of each capacitor in bits. The SMD RF inductors $L_{T1} = L_{T2} = 27\,\text{nH}$ and $L_F = 12\,\text{nH}$ of the type LQW15AN have been used in the demonstrator.

A. SMALL-SIGNAL MEASUREMENT RESULTS

Both quad-band and penta-band prototypes have been measured in free space, the s-parameters for all tuning states have been recorded. The measured 1024 return loss curves at the

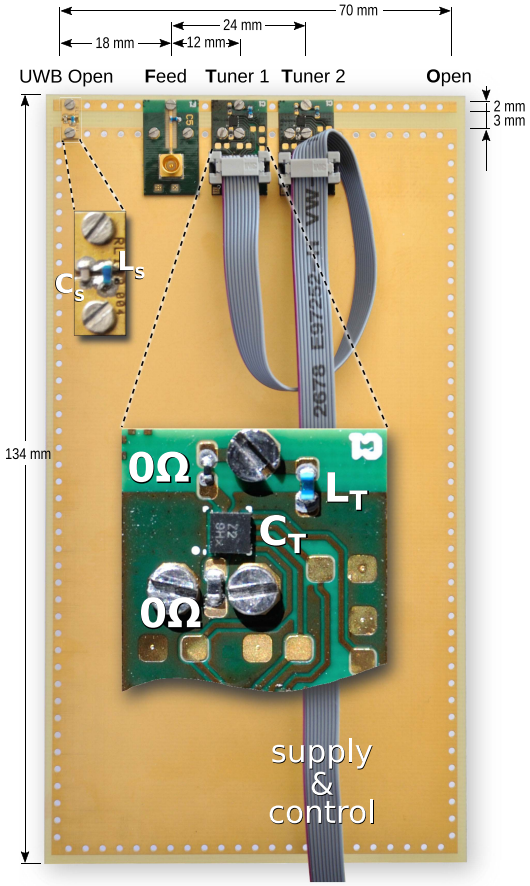

FIGURE 8. Photograph of the assembled hardware demonstrator.

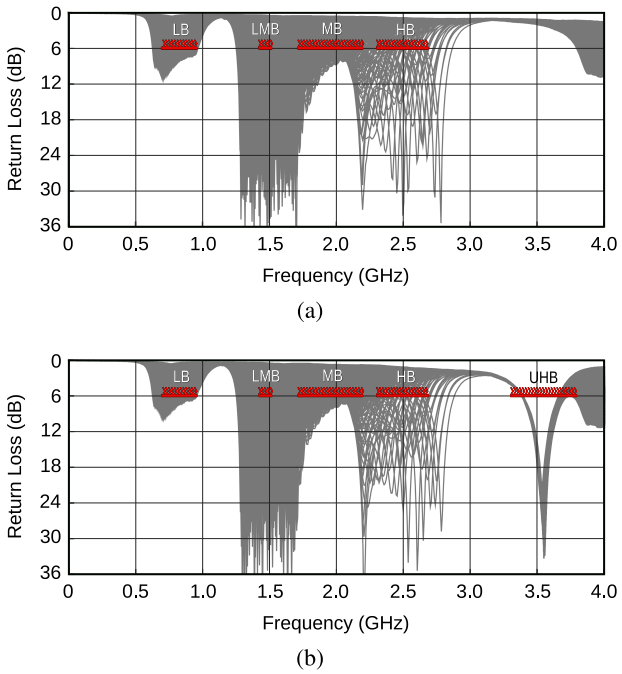

FIGURE 9. Measured return loss of the (a) – quad-band and (b) – penta-band demonstrators in free-space.

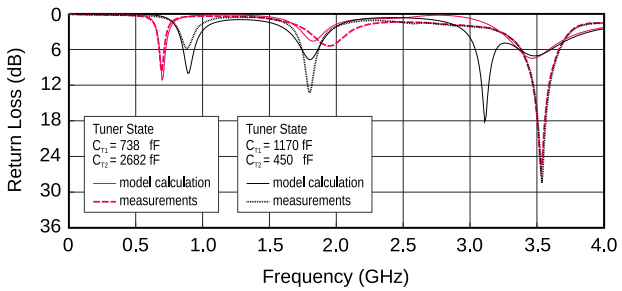

FIGURE 10. Hardware-to-model correlation for penta-band antenna for two tuner states.

RF feed of tuned IFAs are plotted in Fig. 9. 6 dB is set as a commonly adopted return loss target at the feed of antennas integrated into the chassis of cellular phones. As can be observed from the measurements, the proposed tuned IFAs achieve the target return loss for all four frequency bands with fine tuning steps. Only at UHB the return loss overshoots the 6 dB limit at the border of the frequency band. At all bands except HB the curves are merged into a grey shaded area due to their high density.

The curves in Fig. 10 demonstrate the measured versus calculated return loss of the penta-band IFA for two states of the tuning networks. A reasonably good hardware-to-model correlation can be observed, proving the appropriateness of transmission line IFA model at frequencies below one wavelength for the total length of the radiating arm [14]. The discrepancy between the measurements and model prediction at high frequencies is additionally caused by the frequency-dependent electrical parameters of the inductors and switchable capacitors (e.g., increasing capacitance over frequency, finite Q-factor), which were assumed to be ideal in the transmission line model.

In order to demonstrate the capabilities of proposed solution to accommodate for CA application, we have extracted tuner settings suitable for addressing 4 inter-band CA configurations defined in 3GPP Release 11 [13], all located within LB and MB: B8/B3, B5/B3, B5/B1 and B17/B2. Fig. 11 demonstrates the measured return loss curves for aforementioned CA cases with the respective tuner settings. This fits the prediction for simultaneous dual-band coverage capabilities of designed tunable antenna (see Section II-F).

We have not extensively analyzed other CA combinations beyond the presented example due to the high number of band configurations defined in the latest 3GPP releases. However, we believe that if the required CA cases are explicitly specified, the aperture tuning topology (including inductor L_F at the feed) can be optimized to cover all required combinations falling into LB and LMB/MB.

In spite of the strong abstraction and simplicity of the tuned IFA model in Fig. 5(a) and Fig. 6(a), the measurements demonstrate a reasonable hardware-to-model correlation for the return loss at the feed. This proves that the model, in

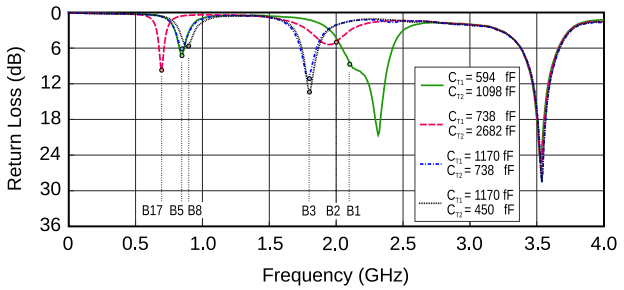

FIGURE 11. Measured return loss of the penta-band antenna for LB-MB carrier aggregation use-cases.

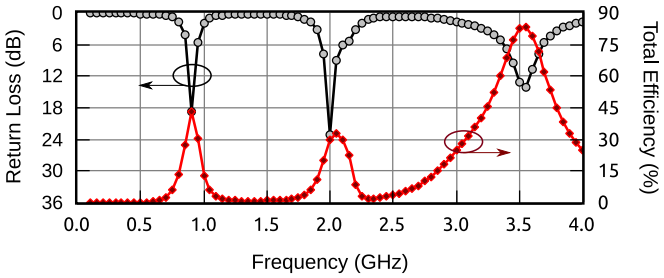

FIGURE 12. Simulated return loss and total antenna efficiency for Band 5 + Band 3 carrier aggregation case (tuner settings $C_{T1} = 1170$ fF, $C_{T2} = 738$ fF).

general, correctly describes the impedance transformation in the antenna and can be used for rapid first-order design of a tunable IFA. The final fine-tuning shall be done on the hardware level, possibly with the help of full-featured EM simulation.

The total antenna efficiency for one state has been simulated in Ansys HFSS. The *measured* responses of the tuning networks in states $C_{T1} = 1170$ fF, $C_{T2} = 738$ fF as well as the UHB open network have been included into the simulation model. The result is demonstrated in Fig. 12. The total efficiency of the antenna is very high at UHB, reaching the peak of over 80 %. At this frequency the antenna tuning networks exhibit very low power losses of below 1 % from the power applied to the feed. This is achieved due to the strong mismatch between the impedance of the aperture tuning networks (which is high at 3.5 GHz) and impedance of the IFA looking into the aperture tuning point (low at 3.5 GHz). For example, the RF voltage magnitudes at tuner 1 and tuner 2 when fed by 1 W signal at 3.5 GHz are 0.43 V and 0.55 V, resulting in power losses of 8 mW and 10 mW respectively. Most of the power is lost on UHB open network, specifically 12 % of the fed power. The efficiency at 900 MHz and 2 GHz is limited to large extent by the power losses in aperture tuning networks operating at high RF voltages, particularly by the first tuner at 2 GHz and by the second one at 900 MHz. It is worth noting, that the total antenna efficiency in the real cellular phone might be lower, especially at UHB, because of many lossy elements and materials in the housing of the device. The radiation patterns at the frequencies corresponding to efficiency peaks are demonstrated in Fig. 13.

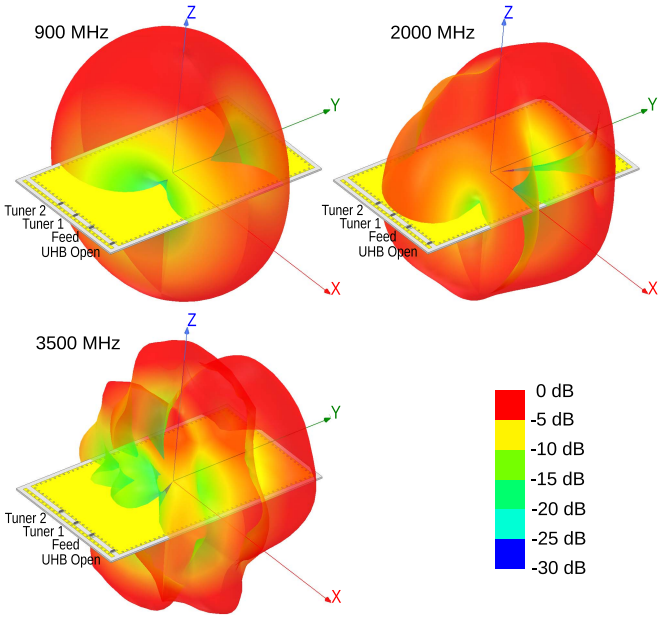

FIGURE 13. Normalized simulated radiation patterns of the penta-band antenna for tuner settings $C_{T1} = 1170$ fF and $C_{T2} = 738$ fF.

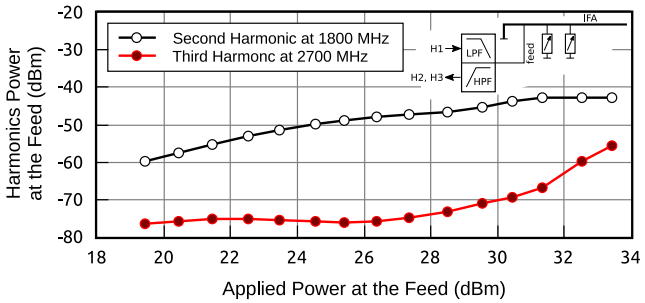

FIGURE 14. Measured harmonics power over applied RF signal at the feed at 900 MHz (tuner settings $C_{T1} = 1170$ fF, $C_{T2} = 738$ fF).

B. LARGE-SIGNAL MEASUREMENT RESULTS

The aperture tuning networks generate nonlinear distortion (e.g., harmonics) when excited by the RF voltage at the IFA. The harmonics power is then radiated by the antenna, coupled back to the IFA feed and dissipated on the lossy elements of the tuning networks and intrinsic IFA.

The measured second and third harmonics at the feed point when driven by the 900 MHz RF signal are plotted in Fig. 14. The peak level of –42 dBm is reached by the second harmonic at 1800 MHz at the feed power of 33 dBm. At this input power level the RF voltage magnitude at the first and second tuners are 45 V and 60 V respectively, meaning that the main generator of the nonlinear distortion in the IFA is the second aperture tuning network.

The radiated harmonics must satisfy the maximum out of band spurious emission requirements of −36 dBm defined by the 3GPP [16] and can be measured over-the-air in dedicated anechoic chamber. Alternatively, they can be estimated by measuring the harmonics at the feed point and scaling the result by the ratio between radiated power and power

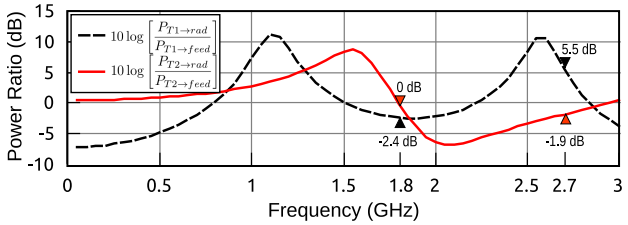

FIGURE 15. Ratio between the radiated harmonic power and harmonic power coupled back to the feed point (tuner settings $C_{T1} = 1170$ fF, $C_{T2} = 738$ fF).

TABLE 3. Comparison of the proposed penta-band IFA with similar tunable single-arm antennas.

Ref.	Bands	Aperture tuner complexity	Note
Single variable capacitor → coverage of up to 3 bands			
[5]	LB or HB	• 1 switchable RF-MEMS cap • 1 fixed SMD cap	Different tuning topologies for each band
[7]	LB, MB	• 1 switchable RF-CMOS cap • 1 fixed SMD inductor	
[9]	LB, LMB, MB HB	• 1 switchable RF-CMOS cap • 1 RF-CMOS switch • 1 fixed SMD cap • 1 fixed SMD inductor	
[10]	LB, MB, HB	• 1 switchable cap • 1 fixed SMD cap	Simulation results only
Two variable capacitors → coverage of up to 5 bands			
This work	LB, LMB, MB, HB	• 2 switchable RF-CMOS caps • 2 fixed SMD inductors	Quad-band configuration
This work	LB, LMB, MB, HB, UHB	• 2 switchable RF-CMOS caps • 3 fixed SMD inductors • 1 fixed SMD cap	Penta-band configuration

dissipated on the feed. The ratio can be obtained from the transmission line model in Fig. 5(a) by applying the voltage at respective aperture tuning point and calculating the amount of power dissipated on the two resistive elements of the circuit R_{RO} and R_{RFFE} [14], with $R_{RFFE} = 50\,\Omega$ being the source resistance of the RF feed:

$$10\log\left[\frac{P_{T1\to rad}}{P_{T1\to feed}}\right] = 10\log\left[\frac{|Z_{T1F}|^2}{|Z_{T1O}|^2}\cdot\frac{\Re\{Z_{T1O}\}}{\Re\{Z_{T1F}\}}\right] \quad (16)$$

$$10\log\left[\frac{P_{T2\to rad}}{P_{T2\to feed}}\right] = 10\log\left[\frac{|Z_{T2F}|^2}{|Z_{T2O}|^2}\cdot\frac{\Re\{Z_{T2O}\}}{\Re\{Z_{T2F}\}}\right] \quad (17)$$

The equations can also be applied to the penta-band antenna as long as the harmonic frequency is below UHB (which is the case for the second and third harmonic of the LB signal). Numerical evaluation of (16) and (17) for the tuner states $C_{T1} = 1170$ fF, $C_{T2} = 738$ fF is shown in Fig. 15. At the frequency of 1800 MHz the difference between the radiated and fed back power of the second harmonic from the 2-nd aperture tuner is 0 dB, meaning that the maximum radiated harmonic power is −42 dBm, which is well below the 3GPP out of band spurious emission limit. Note that for lower frequency of the second harmonic the radiated power may become closer to the emission limit, however, for this case the harmonics measurements at the feed point as well as the numerical evaluation of the ratio between the radiated and fed back harmonic power shall be redone for different state of the aperture tuning networks.

IV. CONCLUSION

The aperture tuning concept based on high-voltage switchable RF capacitors applied to the single-arm IFA is presented in the paper. The IFA can be tuned to any frequency within the five cellular bands in sub-4 GHz range, providing return loss of at least 6 dB at the feed point. The hardware prototype has demonstrated the ability to cover two frequency points at different bands simultaneously. The nonlinear performance fulfills the requirements of the 3GPP for maximum out of band spurious emission, making the proposed concept suitable for practical use.

The comparison of the demonstrated concept with similar tunable IFAs is provided in Table 3. It is worth emphasizing, that the comparison is limited to generic single-arm antenna topologies and does not include solutions based on complex IFA layouts. To authors' knowledge, the proposed penta-band tunable IFA for handheld mobile devices together with the analysis based on the transmission line model is among the simplest solutions reported to date.

REFERENCES

[1] C. R. Rowell and R. D. Murch, "A capacitively loaded PIFA for compact mobile telephone handsets," *IEEE Trans. Antennas Propag.*, vol. 45, no. 5, pp. 837–842, May 1997.
[2] C. S. Park, L. Sundström, A. Wallén, and A. Khayrallah, "Carrier aggregation for LTE-advanced: Design challenges of terminals," *IEEE Commun. Mag.*, vol. 51, no. 12, pp. 76–84, Dec. 2013.
[3] J. Lee *et al.*, "Spectrum for 5G: Global status, challenges, and enabling technologies," *IEEE Commun. Mag.*, vol. 56, no. 3, pp. 12–18, Mar. 2018.
[4] Y. M. Tan, G. H. Ng, and Y. S. R. Tay, "Flexible aperture tuning solution for cellular main antenna in metallic back cover mobile phone," *Adv. Sci. Technol. Eng. Syst. J.*, vol. 2, no. 6, pp. 49–55, 2017.
[5] S. C. Del Barrio, M. Pelosi, G. F. Pedersen, and A. Morris, "Challenges for frequency-reconfigurable antennas in small terminals," in *Proc. IEEE Veh. Technol. Conf. (VTC Fall)*, Sep. 2012, pp. 1–5.
[6] Jing Liang and H. Y. D. Yang, "Frequency reconfigurable printed inverted-F antennas," in *Proc. IEEE Antennas Propagat. Soc. Int. Symp.*, 2008, pp. 1–4.
[7] V. Solomko *et al.*, "Antenna aperture tuning with high-voltage bulk-CMOS switch-based RF capacitor," in *Proc. IEEE Asia-Pac. Microw. Conf. (APMC)*, Dec. 2019, pp. 1464–1466.
[8] T. Houret, L. Lizzi, F. Ferrero, C. Danchesi, and S. Boudaud, "DTC-enabled frequency-tunable inverted-F antenna for IoT applications," *IEEE Antennas Wireless Propag. Lett.*, vol. 19, no. 2, pp. 307–311, Feb. 2020.
[9] H. Hartmann, A. Thomas, V. Solomko, and D. Manteuffel, "Application of a C-tuner to aperture tuning of a handset antenna inspired by characteristic modes," in *Proc. 13th Eur. Conf. Antennas Propag. (EuCAP)*, Mar. 2019, pp. 1–2.
[10] C. Chang, C. Lee, and H. Wang, "Simple tunable inverted-F antenna for LTE/WWAN mobile handset applications," in *Proc. IEEE 5th Asia-Pac. Conf. Antennas Propag. (APCAP)*, Jul. 2016, pp. 401–402.
[11] G. Gonzalez, *Microwave Transistor Amplifiers: Analysis and Design*, 2nd ed. Upper Saddle River, NJ, USA: Prentice Hall, 1997.

[12] S. C. Del Barrio, A. Morris, and G. F. Pedersen, "Antenna miniaturization with MEMS tunable capacitors: Techniques and trade-offs," *Int. J. Antennas Propag.*, vol. 2014, pp. 1–8, Aug. 2014.
[13] "LTE advanced inter-band carrier aggregation (CA) (2DL/1UL), release 11.1.1," 3GPP, Sophia Antipolis, France, Rep. 36.852-11, 2015. Accessed: Jun. 14, 2020. [Online]. Available: https://www.3gpp.org/DynaReport/36852-11.htm
[14] O. Oezdamar, R. Weigel, A. Hagelauer, and V. Solomko, "Considerations for harmonics distribution in aperture-tuned inverted-F antenna for cellular handheld devices," *IEEE Trans. Microw. Theory Techn.*, vol. 68, no. 10, pp. 4122–4130, Oct. 2020.
[15] A. Thomas, W. Bakalski, W. Simbürger, and R. Weigel, "A high quality factor bulk-CMOS switch-based digitally programmable RF capacitor," in *Proc. Asia-Pac. Microw. Conf.*, Nov. 2014, pp. 58–60.
[16] *UTRA (UE) TDD; Radio Transmission and Reception, V1.0.1*, document TSG RAN WG4 S4.02A, 3GPP, Gothenburg, Sweden, 1999. Accessed: Nov. 6, 2020. [Online]. Available: ftp://3gpp.org/tsg_ran/TSG_RAN/TSGR_03/Docs/Pdfs/RP-99278.pdf

VALENTYN SOLOMKO received the B.Sc. and M.Sc. degrees (Hons.) from the National Technical University of Ukraine, Kyiv, Ukraine, and the Ph.D. degree (*summa cum laude*) from the Brandenburg University of Technology, Cottbus, Germany.

From 2009 to 2012, he was with GE Global Research, Munich, Germany, where he was focusing on integrated and discrete electronic solutions for aviation, medical, and industrial applications. In 2012, he joined Infineon Technologies AG, Munich, where he was developing integrated circuits and modules for RF front-ends in mobile handheld devices. He is a Visiting Lecturer with the University of German Federal Armed Forces, Munich, where he is lecturing a course on analog integrated circuit design. He serves as an Associate Editor of IEEE TRANSACTIONS ON MICROWAVE THEORY AND TECHNIQUES.

OGUZHAN OEZDAMAR (Graduate Student Member, IEEE) was born in Fürth, Germany, in 1992. He received the B.Sc. and M.Sc. degrees in electrical engineering from the Friedrich-Alexander-University Erlangen-Nuremberg, Germany, in 2016 and 2018, respectively, where he is currently pursuing the Ph.D. degree.

He is currently a Scientific Assistant with the Institute for Electronics Engineering, Friedrich-Alexander-University Erlangen-Nuremberg. His research interests focus on design and measurement of microwave analog and mixed-signal integrated circuits.

ROBERT WEIGEL (Fellow, IEEE) is currently a Full Professor with the University of Erlangen-Nuremberg, Erlangen, Germany. He co-founded several companies in Germany and Austria, where the Austrian company DICE in Linz was split and overtaken by Infineon and Intel, and Intel sold its company meanwhile to Apple. He has been engaged in microwave electronic circuits and systems and has published more than 1300 articles.

Prof. Weigel received the 2002 VDE ITG-Award, the 2007 IEEE Microwave Applications Award, the 2016 IEEE MTT-S Distinguished Educator Award, the 2018 Distinguished Service Award of the EuMA, the 2018 IEEE Rudolf Henning Distinguished Mentoring Award, and the 2020 IEEE Microwave Career Award. He has been a Distinguished Microwave Lecturer, a MTT-S AdCom Member, and the 2014 MTT-S President. He is a Fellow ITG.

AMELIE HAGELAUER (Senior Member, IEEE) received the Dipl.-Ing. degree in mechatronics and the Dr.-Ing. degree in electrical engineering from Friedrich-Alexander-University Erlangen-Nuremberg, Erlangen, Germany, in 2007 and 2013, respectively.

In November 2007, she joined the Institute for Electronics Engineering, Erlangen, where she was working on thin-film BAW filters toward her Ph.D. degree. Since 2013, she has been focusing on SAW/BAW and RF MEMS components, as well as integrated circuits for frontends up to 180 GHz. From 2016 to 2019, she had been leading a Research Group on Electronic Circuits. She has been a Professor with the University of Bayreuth, Bayreuth, Germany, since August 2019.

Dr. Hagelauer has been the Chair of MTT-2 Microwave Acoustics from 2015 to 2017. She is continuously contributing to the development of the RF Acoustics community by organizing workshops and student design competitions. She has been acting as a Guest Editor for a special issue of the IEEE TRANSACTIONS ON MICROWAVE THEORY AND TECHNIQUES on the topic RF Frontends for Mobile Radio as well as for a special issue in the MDPI Journal *Sensors* on the topic Surface Acoustic Wave and Bulk Acoustic Wave Sensors.